Available online at www.sciencedirect.com
ScienceDirect
Communications in Nonlinear Science and Numerical Simulation 12 (2007) 1560–1571
Communications in Nonlinear Science and Numerical Simulation
www.elsevier.com/locate/cnsns

A numerical method for the Cahn–Hilliard equation with a variable mobility

Junseok Kim *

Department of Mathematics, 103 Multipurpose Science and Technology Building, University of California, Irvine, CA 92697-3875, United States

Received 6 April 2004; received in revised form 7 February 2006; accepted 20 February 2006
Available online 11 May 2006

Abstract

We consider a conservative nonlinear multigrid method for the Cahn–Hilliard equation with a variable mobility of a model for phase separation in a binary mixture. The method uses the standard finite difference approximation in spatial discretization and the Crank–Nicholson semi-implicit scheme in temporal discretization. And the resulting discretized equations are solved by an efficient nonlinear multigrid method. The continuous problem has the conservation of mass and the decrease of the total energy. It is proved that these properties hold for the discrete problem. Also, we show the proposed scheme has a second-order convergence in space and time numerically. For numerical experiments, we investigate the effects of a variable mobility.

PACS: 02.60.Cb; 05.70.Fh

Keywords: Cahn–Hilliard equation; Variable mobility; Nonlinear multigrid method; Phase separation

1. Introduction

In this paper, we consider an efficient and accurate finite difference multigrid approximation of the Cahn–Hilliard (CH) equation with a variable mobility. The quantity $c(\mathbf{x},t)$ is defined to be the mass concentration (volumic mass) of one of the components. The following equation was introduced to model spinodal decomposition and coarsening phenomena in binary alloys [2,6]:

$$\frac{\partial c(\mathbf{x},t)}{\partial t} = \nabla\cdot[M(c(\mathbf{x},t))\nabla\mu(c(\mathbf{x},t))],\quad \mathbf{x}\in\Omega,\ 0<t\leqslant T, \tag{1}$$

$$\mu(c(\mathbf{x},t)) = F'(c(\mathbf{x},t)) - \epsilon^2\Delta c(\mathbf{x},t), \tag{2}$$

* Tel.: +1 949 250 8993.
E-mail address: cfdkim@dongguk.edu
URL: http://math.uci.edu/~jskim/

1007-5704/$ - see front matter
doi:10.1016/j.cnsns.2006.02.010

where $\Omega \subset \mathbf{R}^d$ $(d = 1,2,3)$. This equation arises from the Ginzburg–Landau free energy

$$\mathscr{E}(c) := \int_\Omega \left(F(c) + \frac{\epsilon^2}{2}|\nabla c|^2 \right) \mathrm{d}\mathbf{x},$$

where $F(c)$ is the Helmholtz free energy and ϵ is a positive constant. In this paper, we use the free energy in the form of [10]

$$F(c) = \frac{1}{4}c^2(1-c)^2.$$

To obtain the CH equation with a variable mobility one introduces a chemical potential μ as the variational derivative of $\mathscr{E}$,

$$\mu := \frac{\delta \mathscr{E}}{\delta c} = F'(c) - \epsilon^2 \Delta c$$

and defines the flux, $\mathscr{J} := -M(c)\nabla\mu$, where $M(c) \geqslant 0$ is a diffusional mobility. We take a mobility of the form $M(c) := c(1-c)$, which is a thermodynamically reasonable choice [8]. This mobility significantly lowers the long-range diffusion across bulk regions. As a consequence of mass conservation, we have

$$\frac{\partial c}{\partial t} = -\nabla \cdot \mathscr{J},$$

which is the CH equation with a variable mobility. The natural and no-flux boundary conditions are

$$\frac{\partial c}{\partial n} = \mathscr{J} \cdot n = 0 \quad \text{on } \partial\Omega, \text{ where } n \text{ is normal to } \partial\Omega. \tag{3}$$

We differentiate the energy $\mathscr{E}$ and the total mass $\int_\Omega c\,\mathrm{d}\mathbf{x}$ to get

$$\begin{aligned} \frac{\mathrm{d}}{\mathrm{d}t}\mathscr{E}(t) &= \int_\Omega (F'(c)c_t + \epsilon^2 \nabla c \cdot \nabla c_t)\mathrm{d}\mathbf{x} = \int_\Omega \mu c_t\,\mathrm{d}\mathbf{x} = \int_\Omega \mu \nabla \cdot (M(c)\nabla\mu)\mathrm{d}\mathbf{x} \\ &= \int_{\partial\Omega} \mu M(c)\frac{\partial \mu}{\partial n}\,\mathrm{d}s - \int_\Omega \nabla\mu \cdot (M(c)\nabla\mu)\mathrm{d}\mathbf{x} = -\int_\Omega M(c)|\nabla\mu|^2 \mathrm{d}\mathbf{x} \end{aligned} \tag{4}$$

and

$$\frac{\mathrm{d}}{\mathrm{d}t}\int_\Omega c\,\mathrm{d}\mathbf{x} = \int_\Omega c_t\,\mathrm{d}\mathbf{x} = \int_\Omega \nabla \cdot (M(c)\nabla\mu)\mathrm{d}\mathbf{x} = \int_{\partial\Omega} M(c)\frac{\partial\mu}{\partial n}\,\mathrm{d}s = 0, \tag{5}$$

where we used the no flux boundary condition (3). Therefore, the total energy is non-increasing in time and the total mass is conserved.

The CH equation with a constant mobility has been intensively studied with numerical methods (e.g., [1,3–5,9,11,14], and the references therein). However, only a few authors (e.g., [12,15]) studied the CH equation with concentration dependent mobility numerically, although it appeared in the original derivation of the equation, see [7]. And also, compared to a large number of numerical methods (e.g., a successive overrelaxation iteration method (SOR) [3], a generalized Newton's method [4], and a fast Fourier transformation (FFT) [5]) in solving the CH equation, there is no numerical results by nonlinear multigrid methods to our knowledge, But multigrid methods are generally accepted as among *the fastest numerical methods* for solving this type of partial differential equations [13]. We use a nonlinear multigrid method to solve resulting equations accurately and efficiently.

This paper is organized as follows. In Section 2, we describe the discrete scheme and its properties. We present the nonlinear multigrid method for the fully discrete system in Section 3. In Section 4, a local Fourier analysis of the scheme is performed. The numerical results showing the effects of a variable mobility are described in Section 5. A discussion is presented in Section 6.

2. Numerical analysis

In this section, we present fully discrete schemes for the CH equation. In addition, we prove discrete versions of mass conservation and energy dissipation, which immediately imply the stability of the numerical scheme. We shall first discretize the CH equation (1) and (2) in two-dimensional space, i.e., $\Omega = (a,b)\times(c,d)$. One- and three-dimensional discretizations are analogously defined. Let N_x and N_y be positive even integers, $h = (b-a)/N_x$ be the uniform mesh size, and $\Omega_h = \{(x_i, y_j) : x_i = (i-0.5)h,\ y_j = (j-0.5)h,\ 1 \leqslant i \leqslant N_x,\ 1 \leqslant j \leqslant N_y\}$ be the set of cell-centers.

Let c_{ij} and μ_{ij} be approximations of $c(x_i, y_j)$ and $\mu(x_i, y_j)$. We first implement the zero Neumann boundary condition (3) by requiring that

$$D_x c_{-\frac{1}{2},j} = D_x c_{N_x+\frac{1}{2},j} = D_y c_{i,-\frac{1}{2}} = D_y c_{i,N_y+\frac{1}{2}} = 0,$$

where the discrete differentiation operators are

$$D_x c_{i+\frac{1}{2},j} = \frac{c_{i+1,j} - c_{ij}}{h}, \quad D_y c_{i,j+\frac{1}{2}} = \frac{c_{i,j+1} - c_{ij}}{h}.$$

And we use the notation $\nabla_d c_{ij} = \left(D_x c_{i+\frac{1}{2},j}, D_y c_{i,j+\frac{1}{2}}\right)$ to represent the discrete gradient of c at cell-edges. Correspondingly, the divergence at cell-centers, using values from cell-edges, is $\nabla_d \cdot (g^1, g^2)_{ij} = \left(g^1_{i+\frac{1}{2},j} - g^1_{i-\frac{1}{2},j} + g^2_{i,j+\frac{1}{2}} - g^2_{i,j-\frac{1}{2}}\right)\Big/h$. We then define the discrete Laplacian by $\Delta_d c_{ij} = \nabla_d \cdot \nabla_d c_{ij}$ and the discrete l_2 inner product by

$$(c,d)_h = h^2 \sum_{i=1}^{N_x} \sum_{j=1}^{N_y} c_{ij} d_{ij}, \tag{6}$$

$$(\nabla_d c, \nabla_d d)_e = h^2 \left(\sum_{i=0}^{N_x} \sum_{j=1}^{N_y} D_x c_{i+\frac{1}{2},j} D_x d_{i+\frac{1}{2},j} + \sum_{i=1}^{N_x} \sum_{j=0}^{N_y} D_y c_{i,j+\frac{1}{2}} D_y d_{i,j+\frac{1}{2}} \right). \tag{7}$$

We also define discrete norms as $\|c\|^2 = (c,c)_h$ and $|c|_1^2 = (\nabla_d c, \nabla_d c)_e$.

2.1. Discretization and properties of the proposed scheme

We present a semi-implicit time (Crank–Nicholson) and centered difference space discretization of Eqs. (1) and (2).

$$\frac{c_{ij}^{n+1} - c_{ij}^n}{\Delta t} = \nabla_d \cdot \left[M(c)_{ij}^{n+\frac{1}{2}} \nabla_d \mu_{ij}^{n+\frac{1}{2}} \right], \tag{8}$$

$$\mu_{ij}^{n+\frac{1}{2}} = \frac{1}{2}\left(f(c_{ij}^{n+1}) + f(c_{ij}^n) \right) - \frac{\epsilon^2}{2} \Delta_d (c_{ij}^{n+1} + c_{ij}^n), \tag{9}$$

where $f(c) = F'(c)$ and $\nabla_d \cdot \left[M(c)_{ij}^{n+\frac{1}{2}} \nabla_d \mu_{ij}^{n+\frac{1}{2}} \right]$ is described at (17) in detail. Mass conservation and stability estimate of a discrete energy functional are established in the following theorem and for simplicity, let $M = M(c)^{n+\frac{1}{2}}$.

Theorem 1. *If* $\left\{c^n, \mu^{n+\frac{1}{2}}\right\}$ *is the solution of* (8) *and* (9) *and if we define the discrete energy functional by*

$$\mathscr{E}_h(c^n) = (F(c^n), 1)_h + \frac{\epsilon^2}{2} |c^n|_1^2, \tag{10}$$

then $(c^{n+1}, 1)_h = (c^n, 1)_h$ *and*

$$\mathscr{E}_h(c^{n+1}) - \mathscr{E}_h(c^n) \leqslant -\left(\Delta t - \frac{C\Delta t^2}{h^2}\right)\left(M\nabla_d \mu^{n+\frac{1}{2}}, \nabla_d \mu^{n+\frac{1}{2}}\right)_e.$$

Proof. The first assertion follows using discrete summation by parts. We have

$$(c^{n+1}, 1)_h = (c^n, 1)_h + \Delta t \left(\nabla_d \cdot \left(M \nabla_d \mu^{n+\frac{1}{2}} \right), 1 \right)_h = (c^n, 1)_h - \Delta t \left(M \nabla_d \mu^{n+\frac{1}{2}}, \nabla_d 1 \right)_e = (c^n, 1)_h.$$

It remains to prove the second assertion. Multiplying $\mu^{n+\frac{1}{2}}$ and $c^{n+1} - c^n$ to (8) and (9), respectively and summing by parts, we obtain the following two identities:

$$\left(c^{n+1}-c^n,\mu^{n+\frac{1}{2}}\right)_h+\Delta t\left(M\nabla_d\mu^{n+\frac{1}{2}},\nabla_d\mu^{n+\frac{1}{2}}\right)_e=0, \tag{11}$$

$$\begin{aligned}\left(c^{n+1}-c^n,\mu^{n+\frac{1}{2}}\right)_h&=\frac{1}{2}\left(c^{n+1}-c^n,f(c^{n+1})+f(c^n)\right)_h-\frac{\epsilon^2}{2}\left(c^{n+1}-c^n,\Delta_d c^{n+1}+\Delta_d c^n\right)_h\\&=\frac{1}{2}\left(c^{n+1}-c^n,f(c^{n+1})+f(c^n)\right)_h+\frac{\epsilon^2}{2}\left(|c^{n+1}|_1^2-|c^n|_1^2\right).\end{aligned} \tag{12}$$

Next, using our scheme (8) and (9), we also have the following estimate:

$$\|c^{n+1}-c^n\|^2\leqslant\frac{C\Delta t^2}{h^2}\left\|M\nabla_d\mu^{n+\frac{1}{2}}\right\|^2, \tag{13}$$

where C depends on the dimension of domain of Ω and denotes the generic constant. Indeed, multiplying $c^{n+1}-c^n$ to (8) and using the Hölder inequality, we obtain

$$\|c^{n+1}-c^n\|^2\leqslant\Delta t\|M\nabla_d\mu^{n+\frac{1}{2}}\||c^{n+1}-c^n|_1. \tag{14}$$

On the other hand, the following inequality can be easily verified

$$|c^{n+1}-c^n|_1^2\leqslant\frac{C}{h^2}\|c^{n+1}-c^n\|^2. \tag{15}$$

Combining the above inequalities (14) and (15), we get the estimate (13). Using the identities (11) and (12) above, we obtain

$$\begin{aligned}\mathscr{E}_h(c^{n+1})-\mathscr{E}_h(c^n)&=\left(F(c^{n+1})-F(c^n),1\right)_h+\frac{\epsilon^2}{2}|c^{n+1}|_1^2-\frac{\epsilon^2}{2}|c^n|_1^2\\&=\left(F(c^{n+1})-F(c^n),1\right)_h-\Delta t\left(M\nabla_d\mu^{n+\frac{1}{2}},\nabla_d\mu^{n+\frac{1}{2}}\right)_e-\frac{1}{2}\left(f(c^{n+1})+f(c^n),c^{n+1}-c^n\right)_h.\end{aligned} \tag{16}$$

Since F is differentiable, the first term in right-hand side (16) is estimated as follows:

$$F\left(c^{n+1}\right)-F(c^n)=f\left(\frac{c^{n+1}+c^n}{2}\right)(c^{n+1}-c^n)+\mathrm{O}\left((c^{n+1}-c^n)^2\right).$$

Therefore, using the above identities and estimates we have

$$\begin{aligned}\mathscr{E}_h(c^{n+1})-\mathscr{E}_h(c^n)&\leqslant\left(\frac{F(c^{n+1})-F(c^n)}{c^{n+1}-c^n}-\frac{f(c^{n+1})+f(c^n)}{2},c^{n+1}-c^n\right)_h-\Delta t\left(M\nabla_d\mu^{n+\frac{1}{2}},\nabla_d\mu^{n+\frac{1}{2}}\right)_e\\&=\left(f\left(\frac{c^{n+1}+c^n}{2}\right)-\frac{f(c^{n+1})+f(c^n)}{2}+\mathrm{O}(c^{n+1}-c^n),c^{n+1}-c^n\right)_h-\Delta t\left(M\nabla_d\mu^{n+\frac{1}{2}},\nabla_d\mu^{n+\frac{1}{2}}\right)_e\\&=\left(\mathrm{O}(c^{n+1}-c^n),c^{n+1}-c^n\right)_h-\Delta t\left(M\nabla_d\mu^{n+\frac{1}{2}},\nabla_d\mu^{n+\frac{1}{2}}\right)_e\\&\leqslant\frac{C\Delta t^2}{h^2}\left\|M\nabla_d\mu^{n+\frac{1}{2}}\right\|^2-\Delta t\left(M\nabla_d\mu^{n+\frac{1}{2}},\nabla_d\mu^{n+\frac{1}{2}}\right)_e\leqslant\left(\frac{C\Delta t^2}{h^2}-\Delta t\right)\left(M\nabla_d\mu^{n+\frac{1}{2}},\nabla_d\mu^{n+\frac{1}{2}}\right)_e.\end{aligned}$$

This completes the theorem. □

3. Numerical solution – a nonlinear multigrid method

In this section, we develop a nonlinear full approximation storage (FAS) multigrid method to solve the nonlinear discrete system (8) and (9) at the implicit time level. The nonlinearity is treated using one step of Newton's iteration and a pointwise Gauss–Seidel relaxation scheme is used as the smoother in the multigrid method. See the reference text [13] for additional details and background. The algorithm of the nonlinear multigrid method for solving the discrete CH system is as follows.

First, let us rewrite Eqs. (8) and (9) as

$$\mathrm{NSO}\left(c^{n+1},\mu^{n+\frac{1}{2}}\right)=(\phi^n,\psi^n),$$

where

$$\mathrm{NSO}\left(c^{n+1},\mu^{n+\frac{1}{2}}\right)=\left(\frac{c_{ij}^{n+1}}{\Delta t}-\nabla_d\cdot\left(M(c)_{ij}^{n+\frac{1}{2}}\nabla_d\mu_{ij}^{n+\frac{1}{2}}\right),\mu_{ij}^{n+\frac{1}{2}}-\frac{1}{2}f(c_{ij}^{n+1})+\frac{\epsilon^2}{2}\Delta_d c_{ij}^{n+1}\right)$$

and the source term is

$$(\phi^n,\psi^n)=\left(c_{ij}^n/\Delta t, 0.5f(c_{ij}^n)-0.5\epsilon^2\Delta_d c_{ij}^n\right).$$

In the following description of one FAS cycle, we assume a sequence of grids Ω_k (Ω_{k-1} is coarser than Ω_k by factor 2). Given the number v of pre- and post-smoothing relaxation sweeps, an iteration step for the nonlinear multigrid method using the V-cycle is formally written as follows [13]:

3.1. FAS multigrid cycle

$$\left\{c_k^{m+1},\mu_k^{m+\frac{1}{2}}\right\}=\mathrm{FAS\,cycle}\left(k,c_k^n,c_k^m,\mu_k^{m-\frac{1}{2}},\mathrm{NSO}_k,\phi_k^n,\psi_k^n,v\right).$$

That is, $\left\{c_k^m,\mu_k^{m-\frac{1}{2}}\right\}$ and $\left\{c_k^{m+1},\mu_k^{m+\frac{1}{2}}\right\}$ are the approximations of $c^{n+1}(x_i,y_j)$ and $\mu^{n+\frac{1}{2}}(x_i,y_j)$ before and after an FAS cycle. Now, define the FAS cycle.

(1) Presmoothing:

$$\left\{\bar{c}_k^m,\bar{\mu}_k^{m-\frac{1}{2}}\right\}=\mathrm{SMOOTH}^v\left(c_k^n,c_k^m,\mu_k^{m-\frac{1}{2}},\mathrm{NSO}_k,\phi_k^n,\psi_k^n\right),$$

which means performing v smoothing steps with the initial approximations c_k^m, $\mu_k^{m-\frac{1}{2}}$, c_k^n, source terms ϕ_k^n,ψ_k^n, and SMOOTH relaxation operator to get the approximations $\bar{c}_k^m$, $\bar{\mu}_k^{m-\frac{1}{2}}$. One SMOOTH relaxation operator step consists of solving the system (19) and (20) given below by 2×2 matrix inversion for each i and j. Here, we derive the smoothing operator in two dimensions. Rewriting Eq. (8), we get

$$\frac{c_{ij}^{n+1}}{\Delta t}+\frac{M_{i+\frac{1}{2}j}^{n+\frac{1}{2}}+M_{i-\frac{1}{2}j}^{n+\frac{1}{2}}+M_{i,j+\frac{1}{2}}^{n+\frac{1}{2}}+M_{i,j-\frac{1}{2}}^{n+\frac{1}{2}}}{h^2}\mu_{ij}^{n+\frac{1}{2}}=\phi_{ij}^n+\frac{M_{i+\frac{1}{2}j}^{n+\frac{1}{2}}\mu_{i+1,j}^{n+\frac{1}{2}}+M_{i-\frac{1}{2}j}^{n+\frac{1}{2}}\mu_{i-1,j}^{n+\frac{1}{2}}+M_{i,j+\frac{1}{2}}^{n+\frac{1}{2}}\mu_{i,j+1}^{n+\frac{1}{2}}+M_{i,j-\frac{1}{2}}^{n+\frac{1}{2}}\mu_{i,j-1}^{n+\frac{1}{2}}}{h^2}. \tag{17}$$

Since $f\left(c_{ij}^{n+1}\right)$ is nonlinear with respect to c_{ij}^{n+1}, we linearize $f(c_{ij}^{n+1})$ at c_{ij}^m, i.e.,

$$f(c_{ij}^{n+1})\approx f(c_{ij}^m)+\frac{\mathrm{d}f(c_{ij}^m)}{\mathrm{d}c}(c_{ij}^{n+1}-c_{ij}^m).$$

After substitution of this into (9), we get

$$-\left(\frac{2\epsilon^2}{h^2}+\frac{\mathrm{d}f(c_{ij}^m)}{2\mathrm{d}c}\right)c_{ij}^{n+1}+\mu_{ij}^{n+\frac{1}{2}}=\psi_{ij}^n+\frac{1}{2}f(c_{ij}^m)-\frac{\mathrm{d}f(c_{ij}^m)}{2\mathrm{d}c}c_{ij}^m-\frac{\epsilon^2}{2h^2}\left(c_{i+1,j}^{n+1}+c_{i-1,j}^{n+1}+c_{i,j+1}^{n+1}+c_{i,j-1}^{n+1}\right). \tag{18}$$

Next, we replace c_{kl}^{n+1} and $\mu_{kl}^{n+\frac{1}{2}}$ in Eqs. (17) and (18) with $\bar{c}_{kl}^m$ and $\bar{\mu}_{kl}^{m-\frac{1}{2}}$ if $k\leqslant i$ and $l\leqslant j$, otherwise with c_{kl}^m and $\mu_{kl}^{m-\frac{1}{2}}$, i.e.,

$$\frac{\bar{c}_{ij}^m}{\Delta t}+\frac{M_{i+\frac{1}{2}j}^{m-\frac{1}{2}}+M_{i-\frac{1}{2}j}^{m-\frac{1}{2}}+M_{i,j+\frac{1}{2}}^{m-\frac{1}{2}}+M_{i,j-\frac{1}{2}}^{m-\frac{1}{2}}}{h^2}\bar{\mu}_{ij}^{m-\frac{1}{2}}=\phi_{ij}^n+\frac{M_{i+\frac{1}{2}j}^{m-\frac{1}{2}}\mu_{i+1,j}^{m-\frac{1}{2}}+M_{i-\frac{1}{2}j}^{m-\frac{1}{2}}\bar{\mu}_{i-1,j}^{m-\frac{1}{2}}+M_{i,j+\frac{1}{2}}^{m-\frac{1}{2}}\mu_{i,j+1}^{m-\frac{1}{2}}+M_{i,j-\frac{1}{2}}^{m-\frac{1}{2}}\bar{\mu}_{i,j-1}^{m-\frac{1}{2}}}{h^2}, \tag{19}$$

where $M_{i+\frac{1}{2}j}^{m-\frac{1}{2}}=M\left(\left(c_{ij}^m+c_{i+1,j}^m+c_{ij}^n+c_{i+1,j}^n\right)/4\right)$ and the other terms are similarly defined.

$$-\left(\frac{2\epsilon^2}{h^2}+\frac{\mathrm{d}f(c_{ij}^m)}{2\mathrm{d}c}\right)\bar{c}_{ij}^m+\bar{\mu}_{ij}^{m-\frac{1}{2}}=\psi_{ij}^n+\frac{1}{2}f(c_{ij}^m)-\frac{\mathrm{d}f(c_{ij}^m)}{2\mathrm{d}c}c_{ij}^m-\frac{\epsilon^2}{2h^2}\left(c_{i+1,j}^m+\bar{c}_{i-1,j}^m+c_{i,j+1}^m+\bar{c}_{i,j-1}^m\right). \tag{20}$$

(2) Compute the defect:

$$(\bar{d}_{1k}^{\,m},\bar{d}_{2k}^{\,m})=(\phi_k^n,\psi_k^n)-\mathrm{NSO}_k\left(\bar{c}_k^n,\bar{c}_k^m,\bar{\mu}_k^{m-\frac{1}{2}}\right). \tag{21}$$

(3) Restrict the defect and $\left\{\bar{c}_k^m, \bar{\mu}_k^{m-\frac{1}{2}}\right\}$:

$$\left(\bar{d}_{1k-1}^{\,m}, \bar{d}_{2k-1}^{\,m}\right) = I_k^{k-1}\left(\bar{d}_{1k}^{\,m}, \bar{d}_{2k}^{\,m}\right), \quad \left(\bar{c}_{k-1}^m, \bar{\mu}_{k-1}^{m-\frac{1}{2}}\right) = I_k^{k-1}\left(\bar{c}_k^m, \bar{\mu}_k^{m-\frac{1}{2}}\right).$$

The restriction operator I_k^{k-1} maps k-level functions to $(k-1)$-level functions.

$$d_{k-1}(x_i, y_j) = I_k^{k-1} d_k(x_i, y_j) = \frac{1}{4}\left[d_k\left(x_{i-\frac{1}{2}}, y_{j-\frac{1}{2}}\right) + d_k\left(x_{i-\frac{1}{2}}, y_{j+\frac{1}{2}}\right) + d_k\left(x_{i+\frac{1}{2}}, y_{j-\frac{1}{2}}\right) + d_k\left(x_{i+\frac{1}{2}}, y_{j+\frac{1}{2}}\right)\right].$$

(4) Compute the right-hand side:

$$\left(\phi_{k-1}^n, \psi_{k-1}^n\right) = \left(\bar{d}_{1k-1}^{\,m}, \bar{d}_{2k-1}^{\,m}\right) + \mathrm{NSO}_{k-1}\left(\bar{c}_{k-1}^n, \bar{c}_{k-1}^m, \bar{\mu}_{k-1}^{m-\frac{1}{2}}\right).$$

(5) Compute an approximate solution $\left\{\hat{c}_{k-1}^m, \hat{\mu}_{k-1}^{m-\frac{1}{2}}\right\}$ of the coarse grid equation on Ω_{k-1}, i.e.,

$$\mathrm{NSO}_{k-1}\left(c_{k-1}^n, c_{k-1}^m, \mu_{k-1}^{m-\frac{1}{2}}\right) = \left(\phi_{k-1}^n, \psi_{k-1}^n\right). \tag{22}$$

If $k = 1$, we explicitly invert a 2×2 matrix to obtain the solution. If $k > 1$, we solve (22) by performing a FAS k-grid cycle using $\left\{\bar{c}_{k-1}^m, \bar{\mu}_{k-1}^{m-\frac{1}{2}}\right\}$ as an initial approximation:

$$\left\{\hat{c}_{k-1}^m, \hat{\mu}_{k-1}^{m-\frac{1}{2}}\right\} = \mathrm{FAS\,cycle}\left(k-1, c_{k-1}^n, \bar{c}_{k-1}^m, \bar{\mu}_{k-1}^{m-\frac{1}{2}}, \mathrm{NSO}_{k-1}, \phi_{k-1}^n, \psi_{k-1}^n, v\right).$$

(6) Compute the coarse grid correction (CGC):

$$\hat{v}_{1k-1}^m = \hat{c}_{k-1}^m - \bar{c}_{k-1}^m, \quad \hat{v}_{2k-1}^{m-\frac{1}{2}} = \hat{\mu}_{k-1}^{m-\frac{1}{2}} - \bar{\mu}_{k-1}^{m-\frac{1}{2}}.$$

(7) Interpolate the correction: $\hat{v}_{1k}^m = I_{k-1}^k \hat{v}_{1k-1}^m$, $\hat{v}_{2k}^{m-\frac{1}{2}} = I_{k-1}^k \hat{v}_{2k-1}^{m-\frac{1}{2}}$. Here, the coarse values are simply transferred to the four nearby fine grid points, i.e., $v_k(x_i, y_j) = I_{k-1}^k v_{k-1}(x_i, y_j) = v_{k-1}\left(x_{i+\frac{1}{2}}, y_{j+\frac{1}{2}}\right)$ for i and j odd-numbered integers.

(8) Compute the corrected approximation on Ω_k

$$c_k^{m,\text{after CGC}} = \bar{c}_k^m + \hat{v}_{1k}^{\,m}, \mu_k^{m-\frac{1}{2},\text{after CGC}} = \bar{\mu}_k^{m-\frac{1}{2}} + \hat{v}_{2k}^{\,m-\frac{1}{2}}.$$

(9) Post-smoothing:

$$\left\{c_k^{m+1}, \mu_k^{m+\frac{1}{2}}\right\} = \mathrm{SMOOTH}^v\left(c_k^n, c_k^{m,\text{after CGC}}, \mu_k^{m-\frac{1}{2},\text{after CGC}}, \mathrm{NSO}_k, \phi_k^n, \psi_k^n\right).$$

This completes the description of a nonlinear FAS cycle.

4. Local Fourier analysis

To analyze the behavior of the multigrid method, we linearize the nonlinear scheme and perform a local Fourier analysis (e.g., see [13]). In particular, we analyze the smoother since the performance of the multigrid method depends strongly on the smoother. We "freeze" the coefficient, $M(c)$, at a representative value $M_\xi = M(\xi)$, for some $0 \leqslant \xi \leqslant 1$. After linearizing the nonlinear term $\frac{1}{2}f(c_{ij}^{n+1})$ around an average concentration c_m by $\frac{\alpha}{2}c_{ij}^{n+1} + \beta$, where $\alpha = f'(c_m)$ and β is a constant and substituting $\mu_{ij}^{n+\frac{1}{2}}$ into (8), the scheme becomes

$$L_h c_h^{n+1} = s_h^n, \quad \text{where}$$

$$\begin{aligned} L_h c_h^{n+1} :=& \frac{c_{ij}^{n+1}}{\Delta t M_\xi} - \frac{\alpha}{2h^2}\left(c_{i-1,j}^{n+1} + c_{i+1,j}^{n+1} - 4c_{ij}^{n+1} + c_{i,j-1}^{n+1} + c_{i,j+1}^{n+1}\right) \\ &+ \frac{\epsilon^2}{2h^4}\left[c_{i-2,j}^{n+1} + c_{i+2,j}^{n+1} + c_{i,j-2}^{n+1} + c_{i,j+2}^{n+1} + 2\left(c_{i-1,j+1}^{n+1} + c_{i-1,j-1}^{n+1} + c_{i+1,j+1}^{n+1} + c_{i+1,j-1}^{n+1}\right)\right. \\ &\left. -8\left(c_{i-1,j}^{n+1} + c_{i,j-1}^{n+1} + c_{i+1,j}^{n+1} + c_{i,j+1}^{n+1}\right) + 20c_{ij}^{n+1}\right] \end{aligned} \tag{23}$$

and $s_h^n = \frac{1}{2}\Delta_d f(c_{ij}^n) - \frac{\epsilon^2}{2}\Delta_d^2 c_{ij}^n + \frac{c_{ij}^n}{\Delta t M_\xi}$.

For Gauss–Seidel iteration with a lexicographic ordering of the grid points applied to the above equation (23), we have the following operator decomposition:

$$L_h^+ c_h^{n+1} := \frac{c_{ij}^{n+1}}{\Delta t M_\xi} - \frac{\alpha}{2h^2}\left(c_{i-1,j}^{n+1} + c_{i,j-1}^{n+1} - 4c_{ij}^{n+1}\right)$$
$$+ \frac{\epsilon^2}{2h^4}\left[c_{i-2,j}^{n+1} + c_{i,j-2}^{n+1} + 2\left(c_{i-1,j+1}^{n+1} + c_{i-1,j-1}^{n+1}\right) - 8\left(c_{i-1,j}^{n+1} + c_{i,j-1}^{n+1}\right) + 20c_{ij}^{n+1}\right],$$
$$L_h^- c_h^{n+1} := -\frac{\alpha}{2h^2}\left(c_{i+1,j}^{n+1} + c_{i,j+1}^{n+1}\right) + \frac{\epsilon^2}{2h^4}\left[c_{i+2,j}^{n+1} + c_{i,j+2}^{n+1} + 2\left(c_{i+1,j+1}^{n+1} + c_{i+1,j-1}^{n+1}\right) - 8\left(c_{i+1,j}^{n+1} + c_{i,j+1}^{n+1}\right)\right].$$

Therefore, this relaxation method can be written *locally* as

$$L_h^+ \tilde{z}_h + L_h^- z_h = s_h^n, \tag{24}$$

where z_h corresponds to the old approximation of c_h (approximation before the relaxation step) and $\tilde{z}_h$ to the new approximation (after the step). Subtracting (24) from the discrete equation $L_h c_h = f_h$ and letting $\tilde{v}_h = c_h - \tilde{z}_h$ and $v_h = c_h - z_h$, we obtain the equation

$$L_h^+ \tilde{v}_h + L_h^- v_h = 0, \text{ or, equivalently }, \tilde{v}_h = S_h v_h,$$

where $S_h = -(L_h^+)^{-1} L_h^-$ is the resulting smoothing operator. Applying L_h^+ and L_h^- to the formal eigenfunctions $e^{i\theta_1 x/h} e^{i\theta_2 y/h}$, we obtain

$$L_h^+ e^{\frac{i\theta_1 x}{h}} e^{\frac{i\theta_2 y}{h}} = \widehat{L}_h^+ e^{\frac{i\theta_1 x}{h}} e^{\frac{i\theta_2 y}{h}}, \quad L_h^- e^{\frac{i\theta_1 x}{h}} e^{\frac{i\theta_2 y}{h}} = \widehat{L}_h^- e^{\frac{i\theta_1 x}{h}} e^{\frac{i\theta_2 y}{h}},$$

where $\widehat{L}_h^+$ and $\widehat{L}_h^-$ are the formal eigenvalues of the operators L_h^+ and L_h^-, respectively:

$$\widehat{L}_h^+(\theta_1, \theta_2) = \frac{1}{\Delta t M_\xi} - \frac{\alpha}{2h^2}\left(e^{-i\theta_1} + e^{-i\theta_2} - 4\right)$$
$$+ \frac{\epsilon^2}{2h^4}\left[e^{-2i\theta_1} + e^{-2i\theta_2} + 2\left(e^{-i(\theta_1-\theta_2)} + e^{-i(\theta_1+\theta_2)}\right) - 8\left(e^{-i\theta_1} + e^{-i\theta_2}\right) + 20\right],$$
$$\widehat{L}_h^-(\theta_1, \theta_2) = -\frac{\alpha}{2h^2}\left(e^{i\theta_1} + e^{i\theta_2}\right) + \frac{\epsilon^2}{2h^4}\left[e^{2i\theta_1} + e^{2i\theta_2} + 2\left(e^{i(\theta_1+\theta_2)} + e^{i(\theta_1-\theta_2)}\right) - 8\left(e^{i\theta_1} + e^{i\theta_2}\right)\right].$$

The amplification factor of the relaxation scheme is $\widehat{S}_h(\theta_1, \theta_2) := -\frac{\widehat{L}_h^-(\theta_1, \theta_2)}{\widehat{L}_h^+(\theta_1, \theta_2)}$.

Define the smoothing factor: $\mu_{\mathrm{loc}}(S_h) := \sup\{|\widehat{S}_h(\theta_1, \theta_2)| : \frac{\pi}{2} \leqslant |\theta_1|, |\theta_2| \leqslant \pi\}$.

We define a convergence factor as an average of the quantity $\|d_h^{m+1}\|/\|d_h^m\|$, where d_h^m $(m = 1, 2, \ldots)$ are the defects (21). The convergence factor is estimated numerically using our nonlinear code with the parameters $\epsilon = 0.01$, the mesh-dependent time step $\Delta t = 0.1$ h, and most unstable initial conditions

$$c^0(x, y) = 0.5 + 0.01\cos(0.5\pi x/h)\cos(0.5\pi y/h).$$

We measure the $V(m,n)$-convergence factors, where m and n are the numbers of pre-smoothing and post-smoothing. We focus on $m = 1$ and $n = 1$ as this yields the most efficient algorithms. In addition, we consider $\alpha = -0.25$ which corresponds to linearization in an unstable region. Table 1 shows $\mu_{\mathrm{loc}}(S_h)$ factors with $M_\xi = 0.25$ and measured $\sqrt{V(1,1)}$-cycle convergence factors with different mesh sizes. Note $\sqrt{V(1,1)}$-cycle means the square root of $V(1,1)$-cycle convergence factor. $\sqrt{V(1,1)}$-cycle remains uniformly bounded below 1 with increasing resolutions and apparently converges to a number which is smaller than the theoretical estimate $\mu_{\mathrm{loc}}(S_h)$ as $h \to 0$. This is due to the fact that given a time step, the smoothing factors of coarser grids are

Table 1
Convergence factors for different mesh sizes. $\alpha = -0.25$, $h = 1/N_x$, and $\Delta t = 0.1h$

Case	16×16	32×32	64×64	128×128	256×256	512×512	1024×1024	2048×2048
μ_{loc}	0.2324	0.6083	0.7295	0.6929	0.6763	0.6713	0.6700	0.6697
$\sqrt{V(1,1)}$-cycle	0.1792	0.4299	0.3691	0.3730	0.4104	0.4408	0.4387	0.4340

much smaller than that of the finer one. Thus the number of $V(1,1)$-cycles required to solve the full problem is insensitive to the resolution.

This result for $\alpha = -0.25$ suggests that the multigrid method using a $V(1,1)$-cycle with time step $\Delta t \sim h$ converges uniformly with respect to increasing resolutions. Correspondingly, this would impose a first-order time step constraint on our discrete scheme to solve the CH equation.

5. Numerical results

We consider numerical experiments highlighting the difference between the variable mobility $M(c) = c(1-c)$ and the constant mobility $M(c) \equiv 0.25$ (the maximum value of the variable mobility $M(c)$). We check the second-order convergence of the scheme, demonstrate the total energy dissipation and the mass conservation properties, and study the dynamics of bubbles in the one-, two-, and three-dimensional Cahn–Hilliard equations numerically.

5.1. Convergence test

To obtain an estimate of the rate of convergence, we perform a number of simulations for a sample initial problem on a set of increasingly finer grids. The initial state for this convergence test on a domain, $\Omega = (0,1)\times(0,1)$, is

$$c^0(x,y) = 0.5 + 0.17\cos(\pi x)\cos(2\pi y) + 0.2\cos(3\pi x)\cos(\pi y). \tag{25}$$

The numerical solutions are computed on the uniform grids, $h = 1/2^n$ for $n = 5$, 6, 7, 8, and 9. For each case, the calculation is run to time $T = 0.3$ with the uniform time step, $\Delta t = 0.1$ h, and $\epsilon = 0.01$.

We define the error of a grid to be the discrete l_2-norm of the difference between that grid and the average of the next finer grid cells covering it:

$$e_{h/\frac{h}{2}ij} \stackrel{\text{def}}{=} c_{hij} - \left(c_{\frac{h}{2}2i,2j} + c_{\frac{h}{2}2i-1,2j} c_{\frac{h}{2}2i,2j-1} + c_{\frac{h}{2}2i-1,2j-1}\right)\Big/4.$$

The rate of convergence is defined as the ratio of successive errors: $\log_2 \frac{\|e_{h/\frac{h}{2}}\|}{\|e_{\frac{h}{2}/\frac{h}{4}}\|}$.

The errors and rates of convergence are given in Table 2. The results suggest that the scheme is indeed second-order accurate in space and time.

Next, we compare numerical equilibrium solutions with analytic ones. Fig. 1 shows evolutions of an initial concentration (solid line) $c^0 = 0.5 - 0.3\tanh(5x)$ with three different $\epsilon = 0.01$, 0.02, and 0.04 on a domain $\Omega = (-1,1)$. We take $h = 1/128$ and $\Delta t = 0.1h$. We stop the numerical computations when the discrete l_2-norm of the difference between $(n+1)$th and nth time step solutions becomes less than 10^{-6}. That is $\|c^{n+1} - c^n\| \leqslant 10^{-6}$. Circles are the results of numerical simulations and '$*$', '$+$', and '$\cdot$' are analytic equilibrium solutions [10] $c_{\text{eq}}^{\infty}(x) = \frac{1}{2}\left[1 - \tanh\left(\frac{x}{2\sqrt{2}\epsilon}\right)\right]$ on $\Omega = (-\infty,\infty)$ with $\epsilon = 0.01$, 0.02, and 0.04, respectively. The numerical equilibrium interface profiles match well with the analytical ones.

5.2. The decrease of the total energy

In Fig. 2, the time evolution of the non-dimensional discrete total energy $\mathscr{E}_h(t)/\mathscr{E}_h(0)$ (solid line) and the average concentration $(c^n, 1)_h$ (diamond line) of the numerical solutions with the initial state (26) are shown:

$$c^0(x,y) = 0.3 + 0.1(1 - x - y) + 0.01\text{rand}(). \tag{26}$$

We take the simulation parameters, $\epsilon = 0.01$, $h = 1/64$, $\Delta t = 0.1h$, and mesh size 64×64. The energy is non-increasing and the average concentration is conserved. These numerical results agree well with the total

Table 2
Convergence results – concentration c

Case	32–64	Rate	64–128	Rate	128–256	Rate	256–512
l_2	2.90e−02	2.37	5.61e−03	2.03	1.38e−03	2.01	3.43e−04

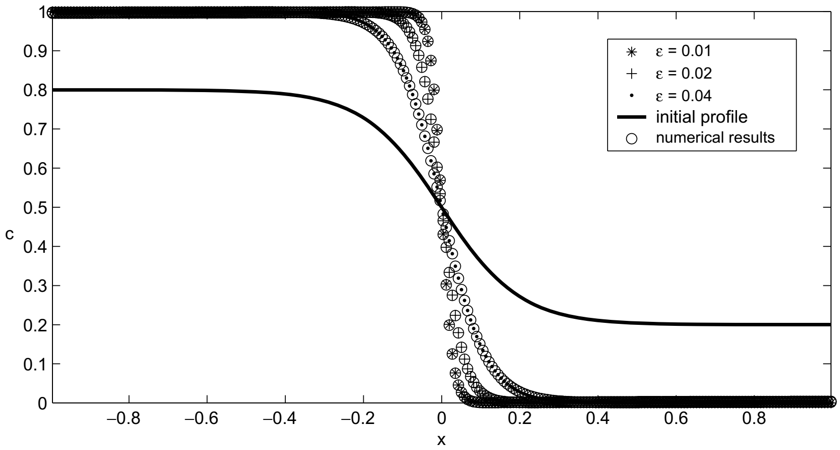

Fig. 1. Circles are numerical equilibrium solutions of an initial concentration $c^0(x) = 0.5 - 0.3\tanh(5x)$ with $\epsilon = 0.01$, 0.02, and 0.04. '$*$', '$+$', and '$\cdot$' are corresponding analytic equilibrium solutions $c_{\mathrm{eq}}^{\infty}(x) = \frac{1}{2}\left[1 - \tanh\left(\frac{x}{2\sqrt{2}\epsilon}\right)\right]$.

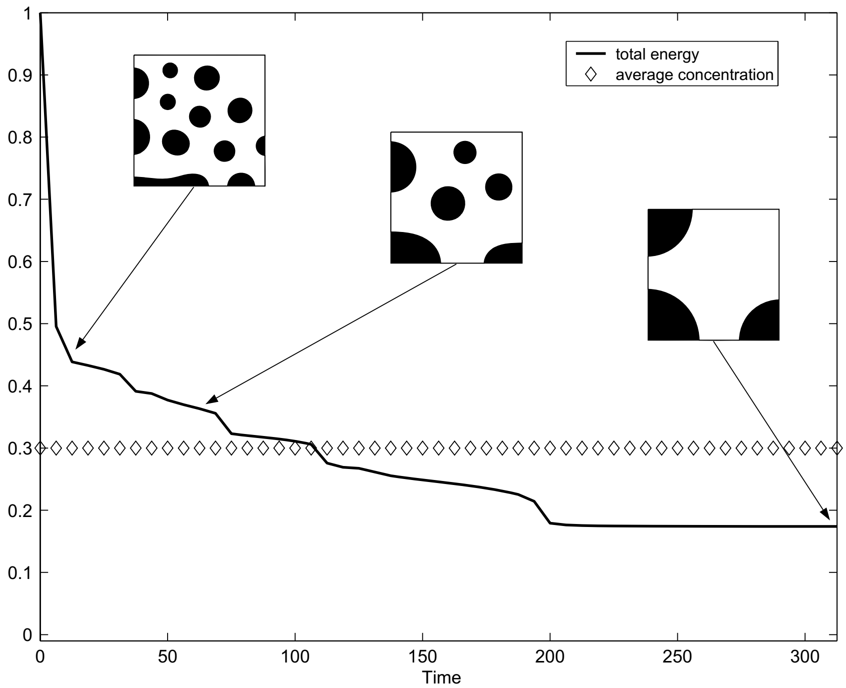

Fig. 2. The non-dimensional discrete total energy $\mathscr{E}_h(t)/\mathscr{E}_h(0)$ (solid line) and the average concentration $(c^n, 1)_h$ (diamond line) of the numerical solutions with the initial state (26).

energy dissipation property (4) and the conservation property (5). Also, the inscribed small figures are the concentration fields at the indicated times.

5.3. One space dimension

Now, we examine the evolution of a random distribution of initial concentration. We take $\epsilon = 0.009$, $h = 1/128$, $\Delta t = 0.2h$, $\Omega = (0, 1)$, and the initial state (dotted line) in Fig. 3 is taken to be $c^0 = 0.3 + 0.01\mathrm{rand}(\,)$. The random number, rand( ), is uniformly distributed between -1 and 1. Fig. 3 shows evolutions of the initial

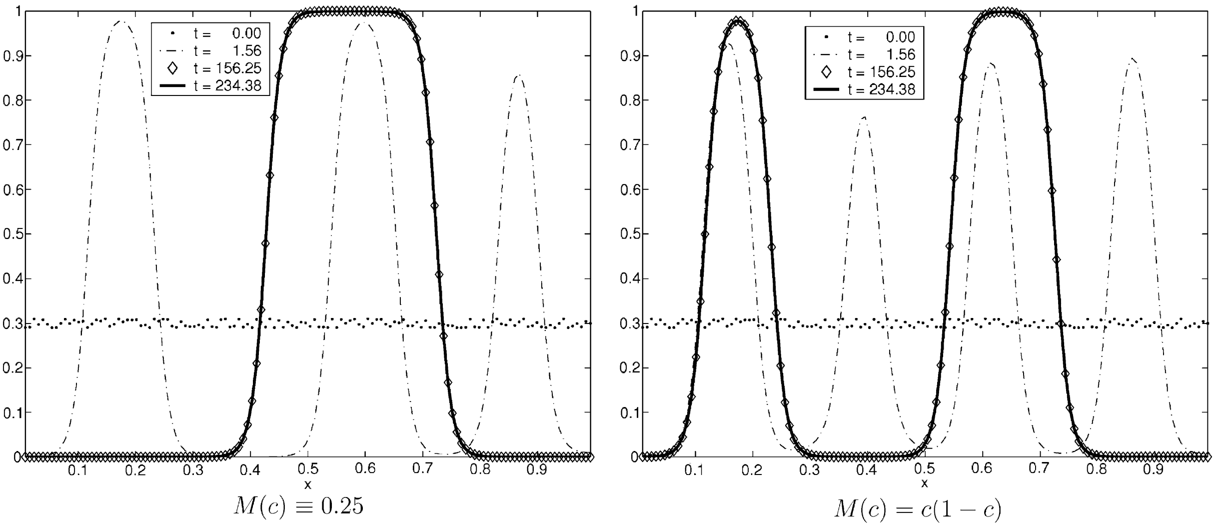

Fig. 3. Evolution of initial concentration $c^0(\cdot) = 0.3 + 0.01\text{rand}()$.

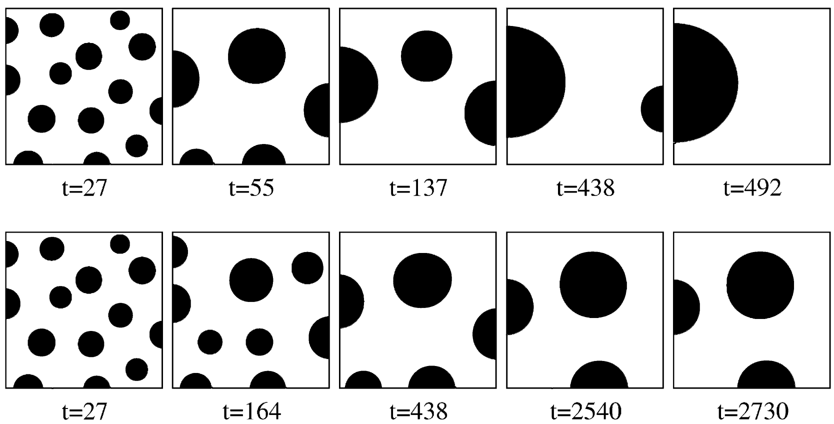

Fig. 4. Evolution of the concentration $c(x, y, t)$ with a constant mobility $M(c) \equiv 0.25$ (the top row) and a variable mobility $M(c) = c(1 - c)$ (the bottom row). The times are shown below each figure.

concentration c^0 with a constant mobility and a variable mobility from a random perturbation. Constant mobility case has only one big component, but the variable mobility case has two components.

5.4. Two space dimensions

In Ref. [12], finite element approximation is used to solve the CH equation with a variable mobility numerically and we take a similar test problem here. The initial state is taken to be $c^0 = 0.25 + 0.001\text{rand}()$. We take the simulation parameters, $\epsilon = 0.004$, $h = 1/128$, $\Delta t = 0.5h$, and mesh size 128×128. Fig. 4 shows evolution of the concentration $c(x, y, t)$ with a constant mobility $M(c) \equiv 0.25$ (the top row) and a variable mobility $M(c) = c(1 - c)$ (the bottom row). In the constant mobility case, the initial data is taken to be $c^0 \equiv c(\cdot, 27)$ from the variable mobility case. The final numerical solutions plotted in Fig. 4 are stationary numerical solutions according to the stopping criteria.

In Fig. 4, in the case of the variable mobility (the bottom row), second-phase regions are nucleated (black regions). The surface energy in the CH equation causes the regions to be circular. There is evidence of a small

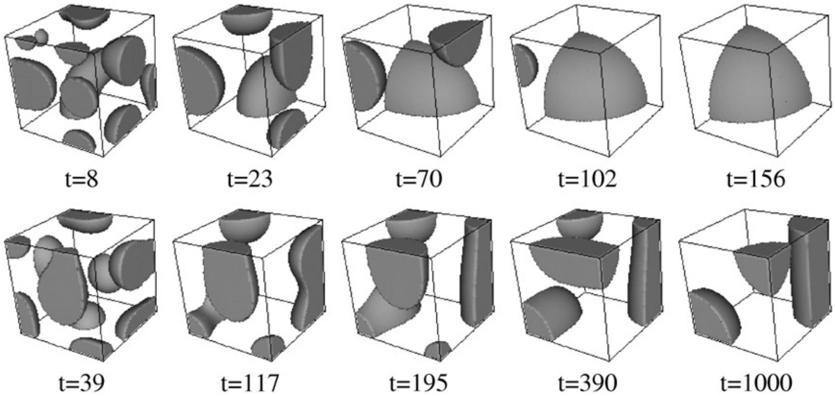

Fig. 5. Evolution of the concentration $c(x,y,z,t)$ with a constant mobility $M(c) \equiv 0.25$ (the top row) and a variable mobility $M(c) = c(1-c)$ (the bottom row). The times are shown below each figure.

amount of coarsening as small regions vanish and redistribute their mass to the other regions. As the remaining regions grow, an equilibrium is established. The variable mobility generally reduces diffusion in the bulk. This is made clear by comparing to the results in the top row, where the mobility is constant. In the case of the constant mobility, the evolution leads to a microstructure consisting entirely of a single large, semi-circular second-phase domain.

5.5. Three space dimensions

We repeat the phase separation simulation in the three-dimensional case. The three-dimensional implementation of the CH equation is a straightforward extension of the two-dimensional one. A $64 \times 64 \times 64$ computational grid, $\epsilon = 0.01$, $h = 1/64$, and $\Delta t = 0.1h$ are used for the numerical parameters. The initial state is taken to be $c^0 = 0.25 + 0.2\text{rand}()$. In Fig. 5, the case of the variable mobility (the bottom row), the numerical stationary solution consists of many components, but the case of the constant mobility (the top row) has only one component.

6. Conclusions

In this paper, an efficient and accurate numerical scheme was proposed for solving the CH equation with a variable mobility. The new scheme is solved by a nonlinear multigrid method and is second-order accurate in space and time. We have studied the dynamics of the one-, two-, and three-dimensional CH equations with a constant mobility and a compositional-dependent mobility. Particularly, we compared the kinetics of bulk-diffusion-controlled coarsening and interface-diffusion-controlled coarsening. We found, in the case of a variable mobility, after the early stages there is very little interaction of regions that do not intersect and the evolution takes place locally where the local mass is preserved. The final frame yields a numerical stationary solution consisting of many components that do not intersect. While, in the case of the constant mobility, diffusion through bulk regions is still possible and disconnected regions influence each other in order to decrease the total amount of interfacial area. For large times, constant mobility CH systems generically lead to situations where each phase occupies only one connected part of the domain.

Acknowledgments

The author thanks his advisor, John Lowengrub, for intellectual and financial support. The author acknowledges the support of the National Science Foundation's Division of Mathematical Sciences. The author also thanks Dr. Hyeong-Gi Lee for very helpful discussions.

References

[1] Bai FS, Spence A, Stuart AM. Numerical computations of coarsening in the one-dimensional Cahn–Hilliard model of phase separation. Physica D 1994;78:155–65.

[2] Cahn JW. On spinodal decomposition. Acta Metall 1961;9:795–801.

[3] Choo SM, Chung SK. Conservative nonlinear difference scheme for the Cahn–Hilliard equation. Comput Math Appl 1998;36:31–9.

[4] Choo SM, Chung SK, Kim KI. Conservative nonlinear difference scheme for the Cahn–Hilliard equation. II. Comput Math Appl 2000;39:229–43.

[5] Copetti M, Elliott CM. Kinetics of phase decomposition processes: numerical solutions to the Cahn–Hilliard equation. Materials Science and Technology 1990;6:273–83.

[6] Cahn JW, Hilliard JE. Free energy of a non-uniform system. I. Interfacial free energy. J Chem Phys 1958;28:258–67.

[7] Cahn JW, Hilliard JE. Spinodal decomposition: A reprise. Acta Metall 1971;19:151–61.

[8] Cahn JW, Taylor JE. Surface motion by surface diffusion. Acta Metall 1994;42:1045–63.

[9] Elliott CM, French DA. Numerical studies of the Cahn–Hilliard equation for phase separation. IMA J Appl Math 1987;38:97–128.

[10] Eggleston JJ, McFadden GB, Voorhees PW. A phase-field model for highly anisotropic interfacial energy. Physica D 2001;150:91–103.

[11] Furihata D. A stable and conservative finite difference scheme for the Cahn–Hilliard Equation. Numer Math 2001;87:675–99.

[12] Barrett JW, Blowey JF, Garcke H. Finite element approximation of the Cahn–Hilliard equation with degenerate mobility. SIAM J Numer Anal 1999;37:286–318.

[13] Trottenberg U, Oosterlee C, Schüller A. Multigrid. Academic press; 2001.

[14] Ye X. The Legendre collocation method for the Cahn–Hilliard equation. J Comput Appl Math 2003;150:87–108.

[15] Zhu J, Chen LQ, Shen J, Tikare V. Coarsening kinetics from a variable mobility Cahn–Hilliard equation – application of semi-implicit Fourier spectral method. Phys Rev E 1999;60:3564–72.